



# NIH Public Access

## Author Manuscript

*Biochemistry*. Author manuscript; available in PMC 2013 August 07.

Published in final edited form as:  
*Biochemistry*. 2012 August 7; 51(31): 6182–6194. doi:10.1021/bi300698h.

## X-ray structures of magnesium and manganese complexes with the N-terminal domain of calmodulin: Insights into the mechanism and specificity of metal ion binding to an EF-hand

F. Timur Senguen and Zenon Grabarek

Boston Biomedical Research Institute, Watertown, MA 02472

### Abstract

Calmodulin (CaM), a member of the EF-hand superfamily, regulates many aspects of the cell function by responding specifically to micromolar concentrations of  $\text{Ca}^{2+}$  in the presence of  $\sim 1000\times$  higher concentration of cellular  $\text{Mg}^{2+}$ . To explain the structural basis of metal ion binding specificity we have solved the X-ray structures of the N-terminal domain of calmodulin (N-CaM) in complexes with  $\text{Mg}^{2+}$ ,  $\text{Mn}^{2+}$  and  $\text{Zn}^{2+}$ . In contrast to  $\text{Ca}^{2+}$ , which induces domain opening in CaM, octahedrally coordinated  $\text{Mg}^{2+}$  and  $\text{Mn}^{2+}$  stabilize the closed-domain, apo-like conformation, while tetrahedrally coordinated  $\text{Zn}^{2+}$  ions bind at the protein surface and do not compete with  $\text{Ca}^{2+}$ . The relative positions of bound  $\text{Mg}^{2+}$  and  $\text{Mn}^{2+}$  within the EF-hand loops are similar to those of  $\text{Ca}^{2+}$ , however the Glu sidechain in the 12<sup>th</sup> position of the loop, whose bidentate interaction with  $\text{Ca}^{2+}$  is critical for domain opening, does not bind directly to either  $\text{Mn}^{2+}$  or  $\text{Mg}^{2+}$  and the vacant ligand position is occupied by a water molecule. We conclude that this critical interaction is prevented by specific stereochemical constraints imposed on the ligands by the EF-hand- $\beta$ -scaffold. The structures suggest that  $\text{Mg}^{2+}$  contributes to the switching off of calmodulin activity and possibly other EF-hand proteins at the resting levels of  $\text{Ca}^{2+}$ . The  $\text{Mg}^{2+}$ -bound N-CaM structure also provides a unique view of a transiently bound hydrated metal ion and suggests a role for the hydration water in the metal induced conformational change.

### Keywords

EF-hand;  $\text{Ca}^{2+}$ -binding; calcium signaling;  $\text{Mg}^{2+}$ -binding; magnesium deficiency; conformational change

---

Transient spikes in the free  $\text{Ca}^{2+}$  concentration activate the function of excitable cells such as myocytes and neurons and regulate a broad range of processes in virtually all cells (1–3). In the resting state the concentration of free  $\text{Ca}^{2+}$  is  $\sim 0.1$  micromolar, and may increase  $\sim 100$  fold upon cell activation. In contrast, the concentration of free  $\text{Mg}^{2+}$  is much higher and remains at a nearly constant level of  $\sim 1.0$  mM (4). Thus,  $\text{Ca}^{2+}$ -signaling occurs in the presence of a large excess of chemically similar divalent cation  $\text{Mg}^{2+}$ . Although  $\text{Mg}^{2+}$  is

---

Address for correspondence: Boston Biomedical Research Institute, 64 Grove Street, Watertown, Massachusetts 02472-2829, Grabarek@BBRI.org, tel: 617-658-7805, fax: 617-972-1753.

#### Supporting information:

**Figure S1.** Determination of  $\text{Ca}^{2+}$ ,  $\text{Mn}^{2+}$  and  $\text{Mg}^{2+}$  binding to N-CaM by isothermal titration calorimetry.

**Figure S2.** Comparison of EF-hand II of the Mg-N-CaM crystal with non-canonical EF-hand structures from calpain and calcyclin.

**Figure S3.** Stabilization of the closed domain conformation in the C-terminal domain of CaM by  $\text{Mg}^{2+}$

**Supplementary video.** Putative steps in the binding of a hydrated  $\text{Mg}^{2+}$  ion ( $\text{Mg}^{2+}(\text{H}_2\text{O})_6$ ) to site II of N-CaM.

This material is available free of charge via the Internet at <http://pubs.acs.org>

**Accession codes.** Coordinates and structure factors for the crystal structures of Mg/Zn-N-CaM, Mg-N-CaM and Mn/Zn-N-CaM are deposited in the Protein Data Bank under accession codes 3UCY, 3UCW, and 3UCT, respectively.

generally considered not to play a regulatory function, large fluxes of Mg<sup>2+</sup> through the cell membrane can be elicited upon hormonal stimulation *in situ* (5–9), which suggests that the free Mg<sup>2+</sup> concentration in cells is tightly regulated. Significant changes in the intracellular free Mg<sup>2+</sup> may occur in some pathological states such as dietary magnesium deficiency (10) or ischemia (11). Several observations point to an antagonistic role of Mg<sup>2+</sup> with respect to Ca<sup>2+</sup> in cell function, however the underlying mechanisms are not well understood. Recently, we put forward a hypothesis that altered Ca<sup>2+</sup> regulation may be an underlying cause of some pathological states attributed to magnesium deficiency (12). Our present work is an attempt at further exploration of this possibility through a detailed structural analysis of Mg<sup>2+</sup> interaction with the key Ca<sup>2+</sup>-sensor protein calmodulin (CaM).

Calmodulin is a member of the EF-hand superfamily of Ca<sup>2+</sup>-binding proteins that function as intracellular receptors of Ca<sup>2+</sup> signals. These proteins change their conformation upon binding Ca<sup>2+</sup>, the property that enables them to regulate the activity of various enzymes in a Ca<sup>2+</sup>-dependent manner (13–15). Many EF-hand proteins also bind Mg<sup>2+</sup> with sufficient affinity to render them fully or partially filled with Mg<sup>2+</sup> at the resting Ca<sup>2+</sup> levels. Thus, the key question is how do these proteins respond specifically to Ca<sup>2+</sup> signals in the presence of ~1000 fold excess of Mg<sup>2+</sup>. Such remarkable functional specificity requires not only a metal ion discrimination based on the binding affinity, but also different structural responses to Ca<sup>2+</sup>-binding vs. Mg<sup>2+</sup>-binding. Even though the Ca<sup>2+</sup>-binding sites in CaM are considered Ca<sup>2+</sup>-specific, they have sufficient affinity for Mg<sup>2+</sup> to be partially occupied by Mg<sup>2+</sup> (possibly as much as 50% in the N-terminal domain) at the resting intracellular Ca<sup>2+</sup> concentrations (16–18) (reviewed in ref (12)). The Ca<sup>2+</sup>-induced activation of CaM requires a transition from a closed-domain to an open-domain conformation in which a target-binding hydrophobic pocket is formed in each of its two domains (19, 20). Mg<sup>2+</sup> ions do not induce domain opening, and thus do not activate CaM (17, 21), but the structural basis for the different conformational response is not well understood.

The metal coordinating ligands in the canonical EF-hand are contained within a 12 amino acid loop, flanked on both ends by  $\alpha$ -helices (22, 23). A pair of EF-hands is required for a structurally stable functional domain. The key element of the domain is a short stretch of antiparallel  $\beta$ -sheet connecting the Ca<sup>2+</sup>-binding loops named “EF-hand- $\beta$ -scaffold”, which was proposed to play an important role in the Ca<sup>2+</sup>-binding mechanism and in the Ca<sup>2+</sup>-induced conformational changes (14, 24). In the proposed model the position of the bound metal ion is defined by the central carbonyl oxygen ligand (the –Y position), a part of the  $\beta$ -scaffold. The ligands in the N-terminal part of the loop are highly mobile and fold readily around the metal ion without significant effects on the domain structure, whereas contribution of a bidentate ligand provided by the side-chain carboxyl group of the invariant Glu residue in the C-terminal (12<sup>th</sup>) position of the loop (Glu<sub>12</sub>) requires a shift of the exiting helix, which opens the domain. The bidentate Ca<sup>2+</sup> coordination by Glu<sub>12</sub> is critical for the domain opening (24, 25) and that interaction is different or missing in the Mg<sup>2+</sup>-EF-hand protein structures. In the Mg<sup>2+</sup>-bound structure of parvalbumin (26) only one oxygen of the Glu<sub>12</sub> side chain interacts with the metal (monodentate ligand) whereas in the structure of calbindin D9k (S100G) Glu<sub>12</sub> does not contact Mg<sup>2+</sup> at all (27) and the vacant coordinating position is occupied by H<sub>2</sub>O (reviewed in (12)). Neither protein undergoes a large conformational change upon Ca<sup>2+</sup>-binding, so it is not possible to make inferences from these structures with respect to CaM. Based on their NMR studies Malmendal and colleagues concluded that Glu<sub>12</sub> does not contribute to Mg<sup>2+</sup> binding in the N-terminal domain of CaM (17, 18) consistent with the closed domain conformation of the Mg<sup>2+</sup>-CaM complex (28). However, the structural basis for that difference is not clear.

Here we report X-ray structures of the N-terminal domain of calmodulin (N-CaM) in complexes with three divalent metal ions: Mg<sup>2+</sup>, Mn<sup>2+</sup> and Zn<sup>2+</sup>. The hexa-coordinated

Mg<sup>2+</sup> and Mn<sup>2+</sup> are bound within the EF-loops whereas the tetra-coordinated Zn<sup>2+</sup> is found only at the interface between N-CaM monomers in the crystal lattice. In these structures N-CaM has a closed-domain apo-like conformation. Characteristically, the last ligand of the Ca<sup>2+</sup>-binding loop (Glu<sub>12</sub>) is not involved in Mg<sup>2+</sup> or Mn<sup>2+</sup> binding, which explains the lack of domain opening and CaM activation by these metal ions. Although like Ca<sup>2+</sup>, both Mg<sup>2+</sup> and Mn<sup>2+</sup> stabilize the N-CaM structure against thermal and urea induced unfolding, the stabilized structures are different. Cumulatively, the presented structures enable us to define the determinants of metal ion specificity in N-CaM. Unexpectedly, one of the structures provides a unique view of a bound hydrated Mg<sup>2+</sup> and suggests that tightly coordinated water molecules may be important for the metal induced conformational transition.

## Materials and Methods

### Protein expression, purification and decalcification

The N-terminal domain of human CaM (residues 1–79) cloned in pAED4 vector (29) was expressed and purified in a similar manner as we previously described for the wild type CaM (20). Briefly, transformed Rosetta cells (Novagen) were grown in 1L of LB at 37 °C. Protein overexpression was induced with 0.1 mM isopropyl-1-thio-β-Dgalactopyranoside when OD<sub>600</sub> reached 0.8–1.0, and the culture was incubated for 3 hours at 37 °C. Cells were harvested via centrifugation (4500 rpm for 15 min at 4 °C) and lysed by freeze-thawing the pellet (3 cycles) suspended in lysis buffer (50 mM Tris pH 8.0, 1 mM EDTA, 0.1 M PMSF). Cell debris was removed via centrifugation (16,000 rpm for 20 min at 4 °C) and the supernatant was brought to 35% saturation of (NH<sub>4</sub>)<sub>2</sub>SO<sub>4</sub> and centrifuged again. The supernatant was filtered through a syringe filter (Whatman, 0.2 µm PVDF w/ GMF) and after addition of 4 mM CaCl<sub>2</sub> applied to a fast flow Phenylsepharose column. The column was then washed with high salt (1 M NaCl, 50 mM Tris pH 8.0, 2 mM CaCl<sub>2</sub>), low salt (0.1 M NaCl, 50 mM Tris pH 8.0, 2 mM CaCl<sub>2</sub>), and medium salt (0.3 M NaCl, 50 mM Tris pH 8.0, 2 mM CaCl<sub>2</sub>) buffers. Purified protein was eluted with 2 mM EDTA (0.3 M NaCl, 50 mM Tris pH 8.0) and the protein containing fractions pooled. The combined fractions were dialyzed against low salt DEAE buffer (50 mM NaCl, 20 mM BisTris pH 6.0) and purified on a DEAE column in a salt gradient (50–500 mM NaCl). Purified N-CaM was dialyzed against 2 mM NH<sub>4</sub>HCO<sub>3</sub> and lyophilized. For crystallization lyophilized protein was dissolved in a minimal amount of 2 mM Hepes pH 7.5 and dialyzed against EDTA buffer (20 mM EDTA with 100 mM NaCl) to ensure decalcification, followed by dialysis against decreasing concentrations of EGTA (20 mM and 0.5 mM EGTA) to maintain a calcium free environment.

### Isothermal titration calorimetry

Metal binding constants were determined via ITC using a VP-ITC calorimeter (MicroCal) and the data analyzed with the program Origin 7 (MicroCal) (30). Decalcified N-CaM samples were dialyzed against ITC buffer (50 mM tris-cacodylate, pH 6.5, 100 mM KCl) and diluted to 20, 20 and 150 µM for titration with CaCl<sub>2</sub>, MnCl<sub>2</sub> and MgCl<sub>2</sub>, respectively. Each protein sample was degassed and immediately used for titration at 22 °C. A series of 10 µl aliquots of 20 fold molar excess of metal relative to total protein concentration were added and the heat due to metal ion binding to N-CaM measured calorimetrically. In each case a total of 300 µl of metal ion solution were added. Each data set was integrated and the resulting plot fitted with a single set of site model using a non-linear least-squares minimization algorithm. The fit parameters were used to calculate the dissociation constant, K<sub>d</sub>, and enthalpy changes, ΔH, due to Ca<sup>2+</sup>, Mn<sup>2+</sup> and Mg<sup>2+</sup> ions binding to N-CaM.

## Thermal unfolding monitored by far UV circular dichroism spectroscopy

Thermal denaturation curves of N-CaM were obtained using an AVIV 62DS CD spectrometer. Protein samples (5  $\mu$ M) in CD Buffer (3M Urea, 10 mM Hepes pH 7.0) were titrated with CaCl<sub>2</sub> (0–1 mM), MnCl<sub>2</sub> (0–10 mM) or MgCl<sub>2</sub> (0–10 mM). Sodium chloride was added as necessary to maintain constant ionic strength of 100 mM. N-CaM samples were denatured from 15–95 °C in 1 degree increments (30 sec equilibration time) and the ellipticity at 222 nm averaged for 5 sec. and recorded. The thermal unfolding curves were fitted as described before to determine melting temperature,  $T_m$ , and heat of unfolding,  $\Delta H$  (31).

## Protein crystallization

All crystals were grown at room temperature using the hanging drop vapor diffusion method with 2  $\mu$ l drops over reservoirs containing 250  $\mu$ l of crystallization solution. N-CaM crystals containing Mn<sup>2+</sup>/Zn<sup>2+</sup> and Mg<sup>2+</sup>/Zn<sup>2+</sup> metal ions were grown from 100 mM Tris-cacodylate pH 6.5, 25 mM ZnCl<sub>2</sub>, 16% PEG8000, 100 mM MnCl<sub>2</sub> or MgCl<sub>2</sub>, and 20% ethylene glycol. Crystal formation under these conditions was complete within a day. Crystals containing only Mg<sup>2+</sup> were grown from 20 mM Tris-cacodylate pH 7.0, 32% PEG8000, 25 mM magnesium acetate, 50 mM KCl, and 25% ethylene glycol. After two days of equilibration, the clear drop was microseeded. All crystals were frozen in liquid nitrogen directly from the crystallization solution.

## X-ray data collection, structure solution and refinement

Data for all crystals were collected at Beamline X29 of the National Synchrotron Light Source (Brookhaven, NY). A complete data set was collected for each crystal at 100 °K at a wavelength of 1.0750 Å. For the Mn/Zn-N-CaM crystal, an additional data set was collected at 1.7587 Å where the anomalous signal due to Mn is stronger than the anomalous signal due to Zn. Reflections were indexed and integrated with DENZO and scaled with SCALEPACK (32). Data from SCALEPACK were then converted into MTZ format with structure factors using the programs ImportScaled and ctruncate, which are included in the CCP4 program suite (33).

SAD phases were determined for Mg/Zn-N-CaM and Mn/Zn-N-CaM using AutoSol module in the Phenix suite (34), using the anomalous signal due to the presence of Zn. The Mg-N-CaM crystal structure was solved using molecular replacement with Phaser-MR and a previously reported apo CaM structure (2PQ3). Electron density maps were improved by creating iterative build composite omit maps using AutoBuild (Phenix) (35). The initial models used for refinement were also created using AutoBuild with the appropriate sequence file for the N-terminal domain of calmodulin.

Initial automatic structural refinement was performed with the program phenix.refine. Metal ions and cacodylate groups were added manually in Coot (36) and ligand restraints produced using ReadySet (Phenix). Following the initial cycle of automatic refinement, several cycles of manual refinement in Coot as well as automatic refinement with phenix.refine and/or refmac5 were performed until R<sub>work</sub> and R<sub>free</sub> had reached acceptable values. Validation of the structure was performed using the Comprehensive Validation option in the Phenix program suite, as well as PROCHECK. Model statistics for each refined crystal structure are compiled in Table 1.

## Results

While both domains of CaM reportedly bind Mg<sup>2+</sup>, the binding to the N-domain is sufficiently strong to significantly affect the regulatory function of CaM under physiological

conditions (17, 18, 37, 38). Therefore our goal was to obtain the high-resolution structure of the Mg<sup>2+</sup>-N-CaM complex. A search for the crystallization conditions using the Hampton Research Crystal Screens I and II yielded tetragonal crystals (space-group P4<sub>3</sub>2<sub>1</sub>2), which contained also Zn<sup>2+</sup> ions in addition to Mg<sup>2+</sup>. Similar crystals of N-CaM obtained in the presence of Zn<sup>2+</sup> only have been previously reported by Warren et al. (39). Upon further search we have obtained triclinic crystals of N-CaM in the presence of Mg<sup>2+</sup> only. The third structure is that of a monoclinic crystal of the Mn<sup>2+</sup>-N-CaM complex also obtained in the presence of Zn<sup>2+</sup>. The three metal ions used in this study have similar ionic radii: 0.72 Å for Mg<sup>2+</sup>, 0.67 Å for Mn<sup>2+</sup> and 0.74 Å for Zn<sup>2+</sup> in the octahedral coordination and 0.60 Å for Zn<sup>2+</sup> in its more common tetrahedral coordination (40). Thus, these metal ions are significantly smaller than Ca<sup>2+</sup> whose ionic radius is 1.00 Å in the octahedral coordination and 1.06 Å in the pentagonal bipyramidal geometry typical for Ca<sup>2+</sup> complexes with EF-hand proteins. Mg<sup>2+</sup> and Mn<sup>2+</sup> prefer octahedral ligand geometry, whereas Zn<sup>2+</sup> has a preference for tetrahedral coordination. The important difference between Mg<sup>2+</sup> and Mn<sup>2+</sup> is that the latter binds N-CaM much more strongly (Table 2, Supplementary Fig. 1). In all the structures described here N-CaM has a closed-domain apo-like conformation, consistent with the fact that none of the three metal ions is able to activate CaM. The structures are described in more detail below.

### Tetragonal crystals Mg/Zn-N-CaM

The Mg<sup>2+</sup>-N-CaM complex forms tetragonal crystals in the presence of Zn<sup>2+</sup> and sodium dimethylarsenate (cacodylate). The structure was solved by molecular replacement using the coordinates of N-CaM structure obtained in the presence of Zn<sup>2+</sup> only (39)(PDB code 2PQ3). Both Ca<sup>2+</sup>-binding loops of N-CaM in the Mg/Zn-N-CaM crystal contain an octahedrally coordinated metal ion. In site II the metal oxygen bond lengths ( $2.18 \pm 0.11$  Å) are consistent with Mg<sup>2+</sup> (41, 42). However, in site I the metal-oxygen bonds ( $2.41 \pm 0.09$  Å) are outside the accepted range for Mg<sup>2+</sup>. The possible candidates are Ca<sup>2+</sup> or Na<sup>+</sup>, for which the average bond lengths found in high-resolution protein structures fall in the same range of 2.35–2.45 Å (42). Calcium is a likely contaminant due to its high affinity for N-CaM, however, modeling the electron density as Ca<sup>2+</sup> resulted in a large negative peak in the Fo-Fc electron density map. Furthermore, the octahedral ligand geometry of the bound metal is inconsistent with the pentagonal bipyramidal geometry of Ca<sup>2+</sup> coordination found in all published CaM structures. Thus, we have concluded that Na<sup>+</sup> is most likely the metal bound at site I. While a relatively strong binding of Na<sup>+</sup> to CaM ( $K_a=230\text{ M}^{-1}$ ) has been detected with <sup>23</sup>Na-NMR (43) it is surprising that Mg<sup>2+</sup> ions did not outcompete Na<sup>+</sup> at this position in the crystal. A significant restriction of the loop conformation due to an interaction with a symmetry related molecule might be responsible. The O<sup>δ</sup> atoms of Asp22 and Asp24 not only coordinate Na<sup>+</sup> but also interact with one of the Zn<sup>2+</sup> ions. The metal ion cluster is further stabilized by the oxygen atoms of dimethylarsenate, which provides a bridge between the two metal ions as well as the same cluster of a symmetry related molecule (39). This leads us to postulate that the absence of Mg<sup>2+</sup> in site I results from unfavorable position of Asp22 and Asp24 side-chains due to the interaction with Zn<sup>2+</sup>.

The Mg<sup>2+</sup> ion bound in site II is octahedrally coordinated by O<sup>δ</sup> atoms of Asp56, Asp58, Asn60 and the carbonyl oxygen of Thr62 (Fig. 1A). The remaining two coordinating positions are occupied by water molecules. The Glu residue in the 12<sup>th</sup> position of the loop (Glu67), which provides bidentate coordination to Ca<sup>2+</sup>, does not interact directly with Mg<sup>2+</sup> ion. The lack of this interaction critical for the Ca<sup>2+</sup>-induced domain opening (24, 25) is, apparently, the reason for the closed-domain conformation of N-CaM in this complex. Importantly, in this structure Mg<sup>2+</sup> occupies the same position as Ca<sup>2+</sup> by directly engaging four of the six ligands that typically are involved in Ca<sup>2+</sup> coordination. Thus, the structure

indicates that Mg<sup>2+</sup> can be a direct competitor with respect to Ca<sup>2+</sup> for site II of CaM depending upon their respective concentrations.

### Triclinic crystals Mg-N-CaM

To resolve the issue of Mg<sup>2+</sup> binding to site I, we have crystallized N-CaM in the presence of Mg<sup>2+</sup> as the sole divalent metal ion. The structure of the Mg<sup>2+</sup>-N-CaM complex reveals three different modes of Mg<sup>2+</sup> interaction with CaM. Two ions are coordinated to the ligands provided by the Ca<sup>2+</sup>-binding loops, whereas the third ion is coordinated by the side-chain carboxyls from adjacent molecules in the crystal lattice. At 1.76 Å resolution (Table 1) all the bound Mg<sup>2+</sup> ions and the interacting ligands, including the tightly coordinated water molecules, are well represented in the electron density map (Fig 1B). The average temperature factor for the bound Mg<sup>2+</sup> is  $26.0 \pm 4.8 \text{ \AA}^2$  (range 20.4–33.8 Å<sup>2</sup>). The asymmetric unit contains four molecules of N-CaM arranged in two pairs. Within each pair the molecules are positioned back-to-back (Fig. 2). This interaction is stabilized by multiple contacts between the helices of site II (helices C and D) and Mg<sup>2+</sup> ion coordinated by the side-chains of Asp64, the residue in the 9<sup>th</sup> position of loop II. The back-to-back interaction of the N-CaM monomers apparently restricts the movement of the helices in EF-hand II, which has some important structural consequences. Each monomer of the Mg<sup>2+</sup>-bound N-CaM has a closed-domain conformation similar to that found in the apo structure, however there are key differences in the position of the helices in site II (see below). The coordination geometry of all Mg<sup>2+</sup> ions in this structure is octahedral. The metal-oxygen bond lengths are in excellent agreement with the expected Mg<sup>2+</sup>-oxygen bond length. In site I, four of the six coordinating positions of the bound Mg<sup>2+</sup> are occupied by the protein ligands that are normally involved in Ca<sup>2+</sup> coordination (side-chain oxygen atoms of Asp20, Asp22, Asp24 and the carbonyl oxygen of Thr26). The two remaining coordinating positions (-X and -Z) are occupied by H<sub>2</sub>O. The position of the bound Mg<sup>2+</sup> ion is the same as that of Ca<sup>2+</sup>, except that the Glu<sub>12</sub> bidentate ligand (Glu31) is not engaged. Thus, this structure shows that site I of N-CaM is fully capable of coordinating the Mg<sup>2+</sup> ion and it supports our earlier conclusion that the lack of Mg<sup>2+</sup> in site I of Mg/Zn-N-CaM crystals resulted from constraints on the ligands (Asp22 and Asp24) due to their simultaneous interaction with Zn<sup>2+</sup>.

Unexpectedly, in site II the Mg<sup>2+</sup> ion is bound in a very different manner (Fig. 1B). The oxygen atom ligands contributed by the protein occupy only two of the six coordinating positions of the Mg<sup>2+</sup> ion. These are the main chain carbonyl oxygen in the – Y position (Thr62), which is a part of the β-scaffold, and the O<sub>γ</sub> of that residue. The remaining 4 coordinating positions are occupied by water molecules. The binding of such a highly hydrated metal ion is strongly stabilized by two-pronged hydrogen bonds of the coordinated water molecules to the side-chain carboxyl oxygen atoms of Asp58 and Glu67, the residues in the 3<sup>rd</sup> and 12<sup>th</sup> position of the loop, respectively, that provide the Y and -Z ligands for Ca<sup>2+</sup> coordination. The entering helix (helix C) is shifted with respect to the β-scaffold in such a way that the side-chain of Asp56, the first residue of the loop (the Ca<sup>2+</sup> ligand in the X position) is spatially too far removed to contact the Mg<sup>2+</sup> ion directly and, instead, forms a hydrogen bond with one of the H<sub>2</sub>O molecules coordinated to the Mg<sup>2+</sup> ion. Thus, although the Mg<sup>2+</sup> ion is coordinated by the ligands of the loop, it still retains most of its hydration water and it has not reached the position normally occupied by Ca<sup>2+</sup>. This structure appears to represent an early step in the metal binding to an EF-hand, which was fortuitously captured due to specific intermolecular contacts in the crystal lattice, specifically the back-to-back interaction of N-CaM monomers (Fig. 2) in both pairs comprising the asymmetric unit of the crystal. The ~3 Å shift of the entering helix is the key difference (Fig. 3). The consequence of this shift is an expansion of the loop (Fig. 4) allowing the almost fully hydrated metal ion to engage the loop ligands. We infer that the

ability of the entering helix to move freely with respect to the  $\beta$ -scaffold is an important factor in the process of metal ion binding. The implications of this unusual mode of metal ion binding will be considered further in the discussion.

### Monoclinic crystals Mn/Zn-N-CaM

Two sets of data were collected from crystals of the  $Mn^{2+}/Zn^{2+}$ -bound form of N-CaM (Table 1). One set collected at 1.054 Å was used for solving and refining the structure, while the second set at 1.7587 Å, close to the anomalous scattering peak of Mn, was used to verify the position of the  $Mn^{2+}$  ions in the structure (Fig. 5). The structure was solved by SAD phasing using anomalous signals of Mn and Zn. The monoclinic crystals (space group P2<sub>1</sub>) contain two N-CaM molecules in the asymmetric unit. Both chains are in the closed-domain conformation and contain  $Mn^{2+}$  ion in each EF-hand loop with identical octahedral ligand geometry. In loop 1 Asp20 provides an axial ligand (X position) to the  $Mn^{2+}$  complex via O<sup>8</sup> with the opposite axial position (-X) occupied by a water molecule. The O<sup>8</sup> atoms of Asp22 and Asp24 provide two equatorial ligands with the backbone carbonyl oxygen atom of Thr26 and a water molecule completing the octahedral ligand geometry. The loop 2 configuration around the second  $Mn^{2+}$  ion is similar. One of the water molecules and the Asp58 O<sup>8</sup> comprise the axial ligands, while the second water molecule, the O<sup>8</sup> atoms of Asp56 and Asn60 and the carbonyl oxygen atom of Thr62 form the equatorial plane of the  $Mn^{2+}$  ligation. Like in the  $Mg^{2+}$ -N-CaM complexes the Glu<sub>12</sub> residues in the -Y coordinating position (Glu31 in site I and Glu67 in site II) do not interact with  $Mn^{2+}$  ion. In chain A, one of the O<sup>e</sup> atoms of this residue coordinates to the exogenous  $Mn^{2+}$  ion exclusive to chain A while the other O<sup>e</sup> atom forms a hydrogen bonding network to the  $Mn^{2+}$  ion in loop 1 via a two water bridge. Alternatively, in chain B one of the Glu31 O<sup>e</sup> atoms forms an indirect bond to the  $Mn^{2+}$  ion in loop 1 via a water bridge involving only a single water molecule.

In addition to the  $Mn^{2+}$  ions,  $Zn^{2+}$  ions from the crystallization milieu were also present, as identified from the anomalous X-ray scattering signal (Fig. 5). The structure presented here includes 4  $Zn^{2+}$  ions, all of which bind at the interface between N-CaM monomers in a tetrahedral geometry. Two of the  $Zn^{2+}$  ions are coordinated by Asp64 and Glu67 on the modeled chains and Glu7 and Glu11 on the symmetry related molecules. The third  $Zn^{2+}$  binds to chain B, residues Asp50 and Glu54, and their symmetry counterparts. The final  $Zn^{2+}$  ion binds on the outside of loop 1 of chain B to two of the same residues that bind  $Mn^{2+}$ , Asp22 and Asp24, but via the alternative O<sup>8</sup> atoms and the O<sup>e</sup> atom of the Glu45 residue on chain A.

It is striking that none of the  $Zn^{2+}$  ions are bound to the  $Ca^{2+}$ -binding loops of N-CaM in a position normally occupied by  $Ca^{2+}$ . This, in principle, could be related to the presence of competing  $Mn^{2+}$  in the Mn/Zn-N-CaM crystals or  $Mg^{2+}$  in the Mg/Zn-N-CaM crystals described above. However,  $Zn^{2+}$  was found not to bind at the  $Ca^{2+}$ -binding sites of N-CaM even in the absence of competing ions (39). A similar observation was reported for the S100 protein interaction with  $Zn^{2+}$  (44). This is surprising in view of the fact that  $Zn^{2+}$  binding to low molecular weight ligands such as EDTA is several orders of magnitude stronger than that of  $Mg^{2+}$ ,  $Ca^{2+}$  or even  $Mn^{2+}$ . According to the Irving-Williams series (45), which compares the stability of various complexes formed by the transition metals,  $Zn^{2+}$  binding to most ligands should be at least equal to, or significantly stronger than that of  $Mn^{2+}$ . This rule is clearly not applicable to the EF-hand  $Ca^{2+}$ -binding sites. A comparison of the N-CaM crystals obtained in the presence of  $Zn^{2+}$  with and without  $Mn^{2+}$  reveals a competition between these metals for the auxiliary sites located at the interface between N-CaM molecules in the crystal lattice, but not for the  $Ca^{2+}$ -binding loops where only  $Mn^{2+}$  ions are found. Apparently the preference for tetrahedral ligand geometry makes  $Zn^{2+}$  incompatible with the ligand geometry in an EF-hand, which can accommodate metal ions in an

octahedral or pentagonal bipyramidal geometry only. Thus,  $Zn^{2+}$  ions cannot compete with  $Ca^{2+}$  for binding to EF-hand proteins.

### Stabilization of the closed domain structure of N-CaM by $Mg^{2+}$

If  $Mg^{2+}$  does not induce domain opening in N-CaM then, does it have any effect on the structure at all? We have addressed this question by measuring the effects of increasing concentrations of  $Mg^{2+}$ ,  $Mn^{2+}$  and  $Ca^{2+}$  on the thermal denaturation of N-CaM. Binding of each of the metal ions tested increased the protein stability as reflected in the increase in unfolding temperature, consistent with the previous report (46). In order to compare directly the effect of  $Mg^{2+}$  vs.  $Ca^{2+}$  we also included 3 M urea in the protein solution, thus lowering the temperature range for the unfolding transition. The increase in the unfolding temperature occurs in a different concentration range for each metal ion, with  $Ca^{2+}$  having the strongest effect (Fig. 6a–c), However, when the melting temperature is plotted as a function of the ratio  $[Me]/K_d$  all three metal ions show similar effect on the stability of N-CaM (Fig. 6d), despite the differences in the domain conformation. The  $Mg^{2+}$ -dependent stabilization of the closed domain conformation has important functional implications: (1) In the absence of  $Ca^{2+}$  it may prevent a partial activation of target enzymes that require the open domain conformation of CaM, and (2) It may promote CaM binding to the group of targets that have a preference for the closed domain conformation, such as those involving the IQ domain. Such a preferential effect of  $Mg^{2+}$  on some model target-CaM interaction has been reported (38).

## Discussion

The closed-domain, apo-like conformation is a common characteristic of the N-CaM structures presented here. The EF-hand loops are extended and the Glu<sub>12</sub> side-chain, whose bidentate interaction with  $Ca^{2+}$  is critical for the domain opening, does not directly contribute to  $Mg^{2+}$  or  $Mn^{2+}$  binding. Cumulatively, our data provide an explanation for the specific functional response of CaM to  $Ca^{2+}$  in the presence of  $Mg^{2+}$ . Unique structural features of the hydrated  $Mg^{2+}$  ion interaction with N-CaM suggest a role for the hydration water in the mechanism of metal binding to an EF-hand and the resultant conformational change.

### Structural basis for the metal ion-dependent functional specificity in a two-EF-hand domain

The structures of the  $Mg^{2+}$ -N-CaM complexes obtained in this work demonstrate that  $Mg^{2+}$  ions compete directly with  $Ca^{2+}$  in both EF-hand loops of N-CaM by engaging the same ligands in all but one coordinating position.  $Mg^{2+}$  fails to directly engage the two side-chain oxygen atoms of Glu<sub>12</sub> and the –Z coordinating position is occupied by H<sub>2</sub>O. In this respect the  $Mg^{2+}$ -N-CaM interaction is similar to that found in site II of the  $Mg^{2+}$ -S100G complex (27). The closed domain conformation and the lack of contribution from Glu<sub>12</sub> are consistent with the NMR data of Malmendal et al.(17), with the lack of hydrophobic site exposure in CaM upon  $Mg^{2+}$  binding (28) and with the lack of enzyme activation by the  $Mg^{2+}$ -CaM complex (21). The high-resolution structures and data presented here offer a view into the underlying mechanism.

The lack of domain opening upon  $Mg^{2+}$  binding to N-CaM can be attributed to several factors, all related in some ways to the smaller ionic radius of  $Mg^{2+}$  as compared to  $Ca^{2+}$ . It is possible that  $Mg^{2+}$  cannot engage the Glu<sub>12</sub> bidentate ligand because the loop cannot contract sufficiently around the smaller  $Mg^{2+}$  ion. This, however, does not appear to play a role since in the structure of  $Mg^{2+}$ -bound parvalbumin (26) the Glu<sub>12</sub> side chain is, in fact, involved in a direct monodentate interaction with  $Mg^{2+}$  (cf. Fig. 3 in ref. (12)). Moreover,

the monodentate interaction is retained even when the side chain is shortened by substitution of Asp for Glu<sub>12</sub>(47). Using molecular dynamics simulations Cates et al. (48) have demonstrated a reversible switching from bidentate to monodentate Glu<sub>12</sub> interaction with the bound metal ion in parvalbumin in response to “alchemical” *in silico* conversion of Ca<sup>2+</sup> into Mg<sup>2+</sup>. The corresponding reduction from five to four oxygen atoms in the equatorial plane of the complex is necessary because the cavity formed by five oxygen atoms is too large for Mg<sup>2+</sup> (cf. discussion and Fig. 3 in ref. (12)). The inability of Glu<sub>12</sub> to engage in a bidentate interaction with Mg<sup>2+</sup> (or Mn<sup>2+</sup>) is also related to the geometric constraints on the bond lengths and bond angles for the bidentate type of carboxylate-metal ion interaction. The smaller the ionic radius the closer the metal ion has to approach to the carboxylate oxygen atoms, which in turn constrains the bond angles. It is not possible to simultaneously satisfy the requirements for bond lengths and bond angles for a bidentate Mg<sup>2+</sup>-carboxylate interaction. While there are examples in the Protein Data Bank of bidentate Mg<sup>2+</sup> coordination by a carboxylate group (Table 3), these structures present a significantly distorted geometry, making their occurrences rare. The preference of Mg<sup>2+</sup> ions for monodentate interaction with carboxylate group is even more striking for small molecule isolated ligands (41) and is well justified by the *ab initio* energy calculations showing that monodentate Mg<sup>2+</sup>-carboxylate interaction is >10 kcal/mol more stable than the bidentate interaction (49).

What remains to be explained is why, in contrast to parvalbumin, in the Mg<sup>2+</sup>-N-CaM complex the Glu<sub>12</sub> side-chain does not contribute any of its oxygen atoms to Mg<sup>2+</sup> coordination, i.e. why a water molecule at the -Z coordinating position is favored over the monodentate coordination by Glu<sub>12</sub>. The explanation is in the different domain conformations of N-CaM and parvalbumin. In parvalbumin the domain comprised of EF-hands II and III is fixed in the open conformation due to its strong interaction with the nonfunctional EF-hand I. The EF-hand helices are in perpendicular orientation in which Glu<sub>12</sub> always remains in a suitable position for interaction with a metal ion. In contrast, in N-CaM the movement of Glu<sub>12</sub> (Glu31 and Glu67) into and out of the metal coordinating position is structurally coupled to a change in the EF-hand interhelical angle associated with the Ca<sup>2+</sup>-induced domain opening (14, 24). The energy of the interaction between Ca<sup>2+</sup> and the two oxygen atoms of Glu<sub>12</sub> must overcome the loss of interhelical hydrophobic contacts associated with domain opening (reviewed by Gifford et al. (15)). Thus, it is plausible that the inability of Glu<sub>12</sub> in N-CaM to bind Mg<sup>2+</sup> results from the lower overall binding energy; the K<sub>d</sub> for Mg<sup>2+</sup> binding to N-CaM is only 0.45 mM as compared to 5.6 μM for Ca<sup>2+</sup> (Table 2). However, this explanation is unsatisfactory in view of the fact that Mn<sup>2+</sup>, which has a similar ionic radius to Mg<sup>2+</sup> but binds N-CaM almost as strongly as Ca<sup>2+</sup> (K<sub>d</sub>=13 μM), also does not engage Glu<sub>12</sub>.

If neither the local metal-ligand interaction geometry nor the overall energy balance can provide adequate explanation for our results, then we are left with the final possibility that the observed ligand-Mg<sup>2+</sup> coordination in N-CaM is a result of some stereochemical constraints specific to the EF-hand. Such constraints are readily understood in light of the EF-hand-β-scaffold mechanism, which attributes a special role to the invariant main chain carbonyl group metal ligand in the -Y coordinating position (12). Unlike other ligands of the EF-hand Ca<sup>2+</sup>-binding loop the -Y carbonyl oxygen is highly constrained due to the strong, polarized hydrogen bonds within the β-scaffold with the pair-mate Ca<sup>2+</sup>-binding loop (50). This, in turn, defines the position of the bound metal ion and, indirectly, limits the available conformational space for the other ligands. The ligands in the N-terminal part of the loop fold around the metal ion due to the flexibility of the main chain, whereas the C-terminal ligand (Glu<sub>12</sub>) moves towards the metal ion together with the exiting helix, which in the case of Ca<sup>2+</sup>, or any metal ion capable of accepting the bidentate coordination, results in the conformational transition. Bidentate coordination of Mg<sup>2+</sup> is geometrically unfavorable, and

a monodentate interaction is energetically insufficient to break the hydrophobic interhelical contacts. As a result, Glu<sub>12</sub> is not engaged in the interaction and a water molecule occupies the vacant ligand position. In view of these considerations we propose that the metal binding specificity of calmodulin, and more importantly its functional specificity, i.e. the ability to be activated specifically by Ca<sup>2+</sup> but not by Mg<sup>2+</sup>, is related primarily to the stereochemical constraints imposed on the metal ligands by the EF-hand-β-scaffold. In view of the fact that all known EF-hand proteins appear to be composed of pairs of EF-hand motives and preserve the EF-hand-β-scaffold structure, it is likely that the above rule is applicable not only to CaM but to any EF-hand protein that has a sufficient affinity for Mg<sup>2+</sup>.

In the context of the above conclusion of particular interest is the potential effect of Mg<sup>2+</sup> on the C-domain of CaM. Obtaining crystals of the Mg<sup>2+</sup>-bound C-domain is technically more challenging due to its lower affinity for Mg<sup>2+</sup> and higher affinity for Ca<sup>2+</sup> as compared to the N-domain (37). However, based on our circular dichroism monitored melting profiles and bisANS fluorescence experiments we conclude that, like in the N-domain, Mg<sup>2+</sup> binding also stabilizes the closed conformation of the C-domain (Supplementary Fig. 3). Although under physiological Mg<sup>2+</sup> concentrations relatively little Mg<sup>2+</sup> binding to the C-domain of free CaM can be expected, the binding may be enhanced in the presence of CaM target molecules with preference for the closed domain conformation, such as the various IQ-domain containing proteins (38). Further studies are needed to fully evaluate the role of Mg<sup>2+</sup> in the cellular function of CaM.

### Potential role of the tightly coordinated water in the metal-dependent conformational transitions in EF-hand proteins

The unusual binding mode of the tetra-hydrated Mg<sup>2+</sup> ion in site II of N-CaM in the Mg<sup>2+</sup>-N-CaM complex provides new insights into the mechanism of metal ion binding to an EF-hand. As the Mn/Zn-N-CaM and Mg/Zn-N-CaM structures show, site II of N-CaM is perfectly competent to coordinate a dehydrated Mg<sup>2+</sup> ion, or its equivalent Mn<sup>2+</sup> ion, deep in the Ca<sup>2+</sup>-binding loop. Yet, that is not the case in the Mg-N-CaM structure. In this structure four of the six coordinating positions of the Mg<sup>2+</sup> ion are still occupied by H<sub>2</sub>O, which clearly is an intermediate state in the process of shedding the hydration water as a part of the binding mechanism. Mg<sup>2+</sup> has unusually high affinity for water, which is responsible for its generally weak interaction with most ligands and proteins. The transport number for Mg<sup>2+</sup>, i.e. an average number of tightly associated water molecules that migrate through the solution as the cation diffuses, is 12–14 (cf. Table 1 in ref. (51)). Six of these water molecules coordinated octahedrally form the first hydration shell, which can be retained in the crystalline state (52). The rate of water exchange from the first hydration shell is more than 1000× slower for Mg<sup>2+</sup> than for Ca<sup>2+</sup> (53). This, exceptionally strong interaction might be one of the reasons why we were able to capture the unusual state of Mg<sup>2+</sup>(H<sub>2</sub>O)<sub>4</sub> bound to an EF-hand. We believe that the structure represents a plausible intermediate state in the binding of Mg<sup>2+</sup>, which occurs when a hydrated ion contacts the loop of an EF-hand (see Supplementary Video).

There are some striking features of the Mg<sup>2+</sup>-N-CaM complex suggesting that binding of other metal ions, Ca<sup>2+</sup> in particular, might occur through a similar intermediate state. CaM and other EF-hand proteins coordinate Ca<sup>2+</sup> ions in a dehydrated form in which only one (or none at all) of the seven coordinating positions retains a water molecule. It is plausible that a transition from the fully hydrated ion in solution to the protein-bound dehydrated form involves some intermediate state(s) similar to that observed in the Mg-N-CaM structure. Such a state, if it occurs, would facilitate the Ca<sup>2+</sup>-induced conformational transition (see below). Here we will highlight the relevant observations: *First*, despite the presence of the hydration water the interaction of Mg<sup>2+</sup>(H<sub>2</sub>O)<sub>4</sub> with site II of N-CaM is very strong mainly due to the double two-pronged, unusually short hydrogen bonds involving the side-chains of

Asp58 (hydrogen bond length =  $2.66 \pm 0.06 \text{ \AA}$ ) and Glu67 (hydrogen bond length =  $2.71 \pm 0.06 \text{ \AA}$ ). Although a similar complex of a hydrated  $\text{Ca}^{2+}$  ion would be significantly less stable due to the much faster solvent exchange rate for  $\text{Ca}^{2+}$  as compared to  $\text{Mg}^{2+}$ (53), it would likely be of sufficient stability to contribute to the transitions between the conformational states of CaM, which are estimated to occur on a microsecond or faster time scale (54–56). *Second*, due to the engagement of the equatorial ligands of the complex in the Y and –Z coordinating positions the hydrated metal ion effectively bridges the opposite sides of the loop. The involvement of the key Glu<sub>12</sub> appears to be of particular importance since it provides a direct link between the metal ion and the exiting helix. It is easy to envision that any change in the position or the hydration state of the bound metal ion in this dynamic complex would have an immediate effect on the exiting helix and could initiate the conformational transition. *Third*, at this early stage of metal-EF-hand interaction, the carbonyl oxygen of the  $\beta$ -scaffold (-Y position) is the only protein ligand whose interaction with the metal ion will remain unchanged in the final complex. Thus, as discussed above, the metal is already properly positioned for the loop to fold around it. *Fourth*, in order to accommodate the hydrated  $\text{Mg}^{2+}$ , the entering helix (helix C) had to be shifted away from the exiting helix (helix D) (Fig. 3). This indicates that such a shift occurs readily without a significant perturbation of the remaining structure. There is evidence that such a shift in EF-hand I of N-CaM may be required for the conformational transition (see below). *Fifth*, the position of the bound  $\text{Mg}^{2+}(\text{H}_2\text{O})_4$  is very similar to that of  $\text{Ca}^{2+}$  in some EF-hand proteins that in the first loop position utilize a main chain carbonyl oxygen as a ligand (Supplementary Fig. 2, cf. ref (14)). This type of  $\text{Ca}^{2+}$  coordination appears to be characteristic of the EF-hand proteins that do not undergo large conformational changes.

Based on the above considerations it seems plausible that the binding of  $\text{Ca}^{2+}$  to EF-hand II of N-CaM may also involve a hydrated ion state analogous to the  $\text{Mg}^{2+}(\text{H}_2\text{O})_4$  state. Is it reasonable to extrapolate this conclusion to site I of N-CaM? The only change in the structure that would be required to accommodate a hydrated  $\text{Ca}^{2+}$  ion in site I of N-CaM is a small shift of helix A on the Z axis of the complex away from helix B. Recent atomistic multi-scale simulations performed by Dupuis and Mousseau (57) provide support for such a process. These authors have investigated the mechanism of domain closing upon  $\text{Ca}^{2+}$  removal from the holo- state of N-domains of calmodulin and troponin C. The main contact between the ends of helices A and B in N-CaM is a highly conserved Phe residue (Phe19), whose bulky hydrophobic side-chain has the unusual property of being more exposed to solvent in the closed-domain apo state than in the open-domain + $\text{Ca}^{2+}$  state. Dupuis and Mousseau have shown that expulsion of Phe19 side chain (or its equivalent in troponin C) from the hydrophobic core is a necessary and limiting step in the domain closing transition (57). Importantly, in each of their successful domain closing trajectories the ends of helices A and B separated transiently to enable the Phe19 side-chain to move out of the hydrophobic core (Normand Mousseau and Lilianne Dupuis, personal communication). The magnitude of such helix separation is similar to that we observe in site II of  $\text{Mg}^{2+}$ -N-CaM. Thus, a transient adjustment of the domain structure that would be required for accommodation of the hydrated  $\text{Ca}^{2+}$  ion might facilitate the conformational transition by permitting Phe19 side-chain to move into the hydrophobic core. This is an attractive concept that adds a dynamic aspect to the EF-hand- $\beta$ -scaffold mechanism and warrants experimental verification.

### Magnesium as a modulator of $\text{Ca}^{2+}$ -signaling in cells

The free  $\text{Mg}^{2+}$  concentration in cells is buffered at a nearly constant level of ~1 mM. For that reason  $\text{Mg}^{2+}$  is unlikely to have a direct regulatory role in cell signaling. However, it is clearly an important player in the  $\text{Ca}^{2+}$ /CaM signaling. As we have shown here  $\text{Mg}^{2+}$  stabilizes the off-state of CaM, thus it can act as a cellular break that counteracts the  $\text{Ca}^{2+}$

activation and facilitates switching off CaM when  $\text{Ca}^{2+}$  concentration returns to resting levels. The effect of  $\text{Mg}^{2+}$  on CaM can be manifested in several ways: (a) Due to the  $\text{Mg}^{2+}/\text{Ca}^{2+}$  competition for the same binding sites the apparent affinity of N-CaM for  $\text{Ca}^{2+}$  is decreased in the presence of  $\text{Mg}^{2+}$ , i.e. the titration curve is shifted to higher  $\text{Ca}^{2+}$  concentrations (18). (b) In systems that involve fast  $\text{Ca}^{2+}$  transients the  $\text{Mg}^{2+}$  dissociation rate may be a limiting factor, i.e. the extent of activation will be inversely related to the  $\text{Mg}^{2+}$  occupancy of N-CaM. Also under the conditions of partial activation when mixed  $\text{Ca}^{2+}/\text{Mg}^{2+}$  species may be formed a different kinetic response may be expected (18). (c) In view of the fact that some targets have a preference for the closed-domain conformation of CaM(58)  $\text{Mg}^{2+}$  may affect the specificity of CaM and its distribution among the cellular targets (38).

$\text{Ca}^{2+}$  signaling in excitable cells such as neurons and myocytes has to be precise in terms of time, space, and amplitude, yet flexible enough to accommodate variable functional demands (1, 59). It appears that changes in  $\text{Mg}^{2+}$  concentration in response to various effectors (6, 60–62) might provide the means to meet such variable demands by finely tuning the response of EF-hand regulated systems including various channel proteins (63, 64).

There are extensive studies documenting a correlation between dietary  $\text{Mg}^{2+}$ -deficiency and various pathological conditions (10) including cardiovascular diseases, hypertension, inflammation, asthma, metabolic syndrome and many others (65–69). Magnesium is the most abundant divalent metal ion in eukaryotic cells and it plays many important cellular functions. However, none of these functions appear to be critically regulated by  $\text{Mg}^{2+}$  in the very narrow concentration range found in magnesium deficiency. We have put forward a hypothesis that EF-hand proteins might be involved and their excessive activation at low  $\text{Mg}^{2+}$  might lead to impaired  $\text{Ca}^{2+}$ -signaling, which in turn, might be a contributing factor in some pathological conditions (12). The structural information obtained in the present work provides a strong support for this hypothesis. Further studies are needed to test the applicability of the rules uncovered here to other EF-hand proteins and to characterize the effects of  $\text{Mg}^{2+}$  on various  $\text{Ca}^{2+}$ -signaling pathways in cells.

## Supplementary Material

Refer to Web version on PubMed Central for supplementary material.

## Acknowledgments

We thank Howard Robinson at the Brookhaven National Laboratory for collecting the synchrotron data at X29 beamline of National Synchrotron Light Source (NSLS). We are grateful to Andrew Bohm, Celia Harrison and Gretchen Meinke of Tufts University for their invaluable help with the initial screening of the crystals on their lab X-ray source. We thank Sam Lehrer, Franklin Fuchs and Andrew Bohm for critical comments on the manuscript.

Funding information:

This work was supported by the National Institutes of Health (grant HL91162).

## Abbreviations

<b>CaM</b>	recombinant human calmodulin
<b>N-CaM</b>	recombinant N-terminal fragment of calmodulin (residues 1–79)
<b>C-CaM</b>	recombinant C-terminal fragment of calmodulin (residues 79–148)
<b>ITC</b>	isothermal titration microcalorimetry

**CD** circular dichroism

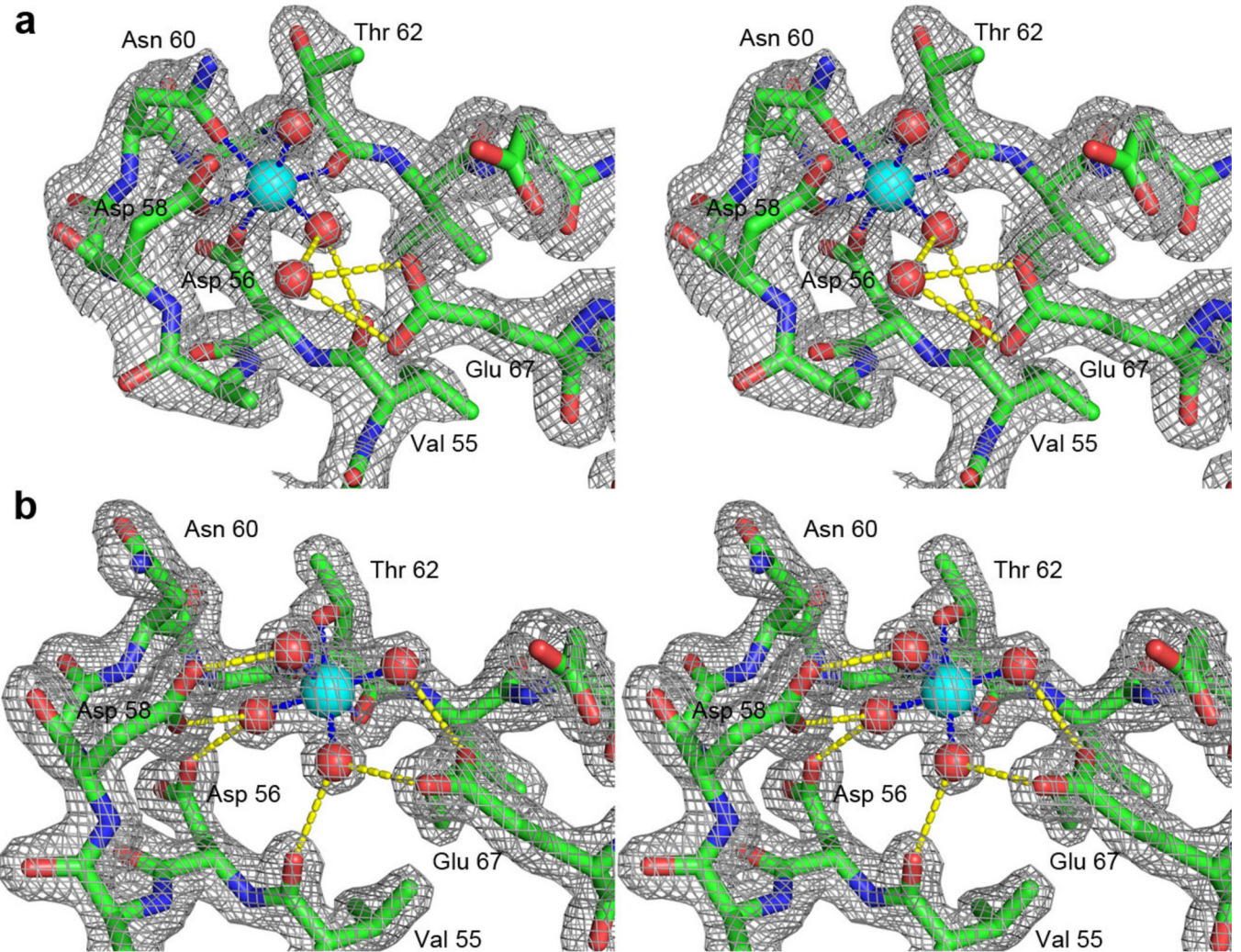
## References

1. Berridge MJ, Lipp P, Bootman MD. The versatility and universality of calcium signalling. *Nat Rev Mol Cell Biol.* 2000; 1:11–21. [PubMed: 11413485]
2. Carafoli E, Santella L, Branca D, Brini M. Generation, control, and processing of cellular calcium signals. *Crit Rev Biochem Mol Biol.* 2001; 36:107–260. [PubMed: 11370791]
3. Clapham DE. Calcium signaling. *Cell.* 2007; 131:1047–1058. [PubMed: 18083096]
4. Romani A, Scarpa A. Regulation of cell magnesium. *Arch Biochem Biophys.* 1992; 298:1–12. [PubMed: 1524417]
5. Romani A, Scarpa A. Hormonal control of Mg<sup>2+</sup> transport in the heart. *Nature.* 1990; 346:841–844. [PubMed: 2168019]
6. Romani A, Marfella C, Scarpa A. Regulation of magnesium uptake and release in the heart and in isolated ventricular myocytes. *Circ Res.* 1993; 72:1139–1148. [PubMed: 8495544]
7. Fatholahi M, LaNoue K, Romani A, Scarpa A. Relationship between total and free cellular Mg(2+) during metabolic stimulation of rat cardiac myocytes and perfused hearts. *Arch Biochem Biophys.* 2000; 374:395–401. [PubMed: 10666323]
8. Keenan D, Romani A, Scarpa A. Regulation of Mg<sup>2+</sup> homeostasis by insulin in perfused rat livers and isolated hepatocytes. *FEBS Lett.* 1996; 395:241–244. [PubMed: 8898104]
9. Romani AM, Maguire ME. Hormonal regulation of Mg<sup>2+</sup> transport and homeostasis in eukaryotic cells. *Biometals.* 2002; 15:271–283. [PubMed: 12206393]
10. Seelig, MS. Magnesium deficiency in the pathogenesis of disease. Early roots of cardiovascular, Skeletal and renal abnormalities. New York, NY: Goldwater Memorial Hospital, New York University Medical Center; 1980.
11. Harkema JM, Chaudry IH. Magnesium-adenosine triphosphate in the treatment of shock, ischemia, and sepsis. *Crit Care Med.* 1992; 20:263–275. [PubMed: 1737460]
12. Grabarek Z. Insights into modulation of calcium signaling by magnesium in calmodulin, troponin C and related EF-hand proteins. *Biochimica et Biophysica Acta (BBA) - Molecular Cell Research.* 2011; 1813:913–921.
13. Crivici A, Ikura M. Molecular and structural basis of target recognition by calmodulin. [Review]. *Annual Review of Biophysics & Biomolecular Structure.* 1995; 24:85–116.
14. Grabarek Z. Structural basis for diversity of the EF-hand calcium-binding proteins. *J Mol Biol.* 2006; 359:509–525. [PubMed: 16678204]
15. Gifford JL, Walsh MP, Vogel HJ. Structures and metal-ion-binding properties of the Ca<sup>2+</sup>-binding helix-loop-helix EF-hand motifs. *Biochem J.* 2007; 405:199–221. [PubMed: 17590154]
16. Ohki SY, Ikura M, Zhang MJ. Identification of Mg<sup>2+</sup>-Binding Sites and the Role of Mg<sup>2+</sup> on Target Recognition By Calmodulin. *Biochemistry.* 1997; 36:4309–4316. [PubMed: 9100027]
17. Malmendal A, Evenas J, Thulin E, Gippert GP, Drakenberg T, Forsen S. When size is important. Accommodation of magnesium in a calcium binding regulatory domain. *J Biol Chem.* 1998; 273:28994–29001. [PubMed: 9786904]
18. Malmendal A, Linse S, Evenas J, Forsen S, Drakenberg T. Battle for the EF-hands: magnesium–calcium interference in calmodulin. *Biochemistry.* 1999; 38:11844–11850. [PubMed: 10512641]
19. Zhang M, Tanaka T, Ikura M. Calcium-induced conformational transition revealed by the solution structure of apo calmodulin. *Nature Structural Biology.* 1995; 2:758–767.
20. Tan RY, Mabuchi Y, Grabarek Z. Blocking the Ca<sup>2+</sup>-induced conformational transitions in calmodulin with disulfide bonds. *J. Biol. Chem.* 1996; 271:7479–7483. [PubMed: 8631777]
21. Chao SH, Suzuki Y, Zysk JR, Cheung WY. Activation of calmodulin by various metal cations as a function of ionic radius. *Mol Pharmacol.* 1984; 26:75–82. [PubMed: 6087119]
22. Kretsinger RH, Nockolds CE. Carp muscle calcium binding protein. II. Structure determination and general description. *J. Biol. Chem.* 1973; 248:3313–3326. [PubMed: 4700463]

23. Strynadka NCJ, James MNG. Crystal structures of the helix-loop-helix calcium-binding proteins. *Annu. Rev. Biochem.* 1989; 58:951–998. [PubMed: 2673026]
24. Grabarek Z. Structure of a trapped intermediate of calmodulin: calcium regulation of EF-hand proteins from a new perspective. *J Mol Biol.* 2005; 346:1351–1366. [PubMed: 15713486]
25. Gagne SM, Li MX, Sykes BD. Mechanism Of Direct Coupling Between Binding and Induced Structural Change In Regulatory Calcium Binding Proteins. *Biochemistry.* 1997; 36:4386–4392. [PubMed: 9109645]
26. Declercq JP, Tinant B, Parello J, Rambaud J. Ionic interactions with parvalbumins. Crystal structure determination of pike 4.10 parvalbumin in four different ionic environments. *J Mol Biol.* 1991; 220:1017–1039. [PubMed: 1880797]
27. Andersson M, Malmendal A, Linse S, Ivarsson I, Forsen S, Svensson LA. Structural basis for the negative allosteric between Ca(2+)- and Mg(2+)- binding in the intracellular Ca(2+)-receptor calbindin D9k. *Protein Sci.* 1997; 6:1139–1147. [PubMed: 9194174]
28. Follenius A, Gerard D. Fluorescence investigations of calmodulin hydrophobic sites. *Biochem Biophys Res Commun.* 1984; 119:1154–1160. [PubMed: 6324780]
29. Doering DS, Matsudaira P. Cysteine Scanning Mutagenesis At 40 Of 76 Positions In Villin Headpiece Maps the F-Actin Binding Site and Structural Features Of the Domain. *Biochemistry.* 1996; 35:12677–12685. [PubMed: 8841111]
30. Wiseman T, Williston S, Brandts JF, Lin LN. Rapid measurement of binding constants and heats of binding using a new titration calorimeter. *Anal Biochem.* 1989; 179:131–137. [PubMed: 2757186]
31. Meyer DF, Mabuchi Y, Grabarek Z. The role of Phe-92 in the Ca2+-induced conformational transition in the C-terminal domain of calmodulin. *J. Biol. Chem.* 1996; 271:11284–11290. [PubMed: 8626680]
32. Otwinowski Z, Minor W. Processing of X-ray diffraction data collected in oscillation mode. *Methods Enzymol.* 1997; 276:307–326.
33. Collaborative Computational Project, n. The CCP4 suite: programs for protein crystallography. *Acta Crystallographica Section D.* 1994; 50:760–763.
34. Adams PD, Grosse-Kunstleve RW, Hung LW, Ioerger TR, McCoy AJ, Moriarty NW, Read RJ, Sacchettini JC, Sauter NK, Terwilliger TC. PHENIX: building new software for automated crystallographic structure determination. *Acta Crystallogr D Biol Crystallogr.* 2002; 58:1948–1954. [PubMed: 12393927]
35. Terwilliger TC, Grosse-Kunstleve RW, Afonine PV, Moriarty NW, Adams PD, Read RJ, Zwart PH, Hung L-W. Iterative-build OMIT maps: map improvement by iterative model building and refinement without model bias. *Acta Crystallographica Section D.* 2008; 64:515–524.
36. Emsley P, Cowtan K. Coot: model-building tools for molecular graphics. *Acta Crystallogr D Biol Crystallogr.* 2004; 60:2126–2132. [PubMed: 15572765]
37. Tsai MD, Drakenberg T, Thulin E, Forsen S. Is the binding of magnesium (II) to calmodulin significant? An investigation by magnesium-25 nuclear magnetic resonance. *Biochemistry.* 1987; 26:3635–3643. [PubMed: 3651401]
38. Martin SR, Masino L, Bayley PM. Enhancement by Mg<sup>2+</sup> of domain specificity in Ca<sup>2+</sup>-dependent interactions of calmodulin with target sequences. *Protein Sci.* 2000; 9:2477–2488. [PubMed: 11206069]
39. Warren JT, Guo Q, Tang WJ. A 1.3-A structure of zinc-bound N-terminal domain of calmodulin elucidates potential early ion-binding step. *J Mol Biol.* 2007; 374:517–527. [PubMed: 17942116]
40. Shannon RD. Revised effective ionic radii and systematic studies of interatomic distances in halides and chalcogenides. *Acta Crystallogr A.* 1976; 32:751–767.
41. Carrell CJ, Carrell HL, Erlebacher J, Glusker JP. Structural aspects of metal-ion carboxylate interactions. *Journal of the American Chemical Society.* 1988; 110:8651–8656.
42. Harding MM. Small revisions to predicted distances around metal sites in proteins. *Acta Crystallogr D Biol Crystallogr.* 2006; 62:678–682. [PubMed: 16699196]
43. Delville A, Grandjean J, Laszlo P, Gerday C, Brzeska H, Drabikowski W. Sodium-23 nuclear magnetic resonance as an indicator of sodium binding to calmodulin and tryptic fragments, in relation to calcium content. *Eur J Biochem.* 1980; 109:515–522. [PubMed: 7408898]

44. Moroz OV, Blagova EV, Wilkinson AJ, Wilson KS, Bronstein IB. The crystal structures of human S100A12 in apo form and in complex with zinc: new insights into S100A12 oligomerisation. *J Mol Biol.* 2009; 391:536–551. [PubMed: 19501594]
45. Irving H, Williams RJP. The stability of transition-metal complexes. *Journal of the Chemical Society.* 1953:3192–3210.
46. Brzeska H, Venyaminov SV, Grabarek Z, Drabikowski W. Comparative studies on thermostability of calmodulin, skeletal muscle troponin C and their tryptic fragments. *FEBS Lett.* 1983; 153:169–173. [PubMed: 6825857]
47. Cates MS, Berry MB, Ho EL, Li Q, Potter JD, Phillips GN Jr. Metal-ion affinity and specificity in EF-hand proteins: coordination geometry and domain plasticity in parvalbumin. *Structure Fold Des.* 1999; 7:1269–1278. [PubMed: 10545326]
48. Cates MS, Teodoro ML, Phillips GN Jr. Molecular mechanisms of calcium and magnesium binding to parvalbumin. *Biophys J.* 2002; 82:1133–1146. [PubMed: 11867433]
49. Deerfield DW 2nd, Fox DJ, Head-Gordon M, Hiskey RG, Pedersen LG. The first solvation shell of magnesium ion in a model protein environment with formate, water, and X-NH<sub>3</sub>, H<sub>2</sub>S, imidazole, formaldehyde, and chloride as ligands: an Ab initio study. *Proteins.* 1995; 21:244–255. [PubMed: 7784428]
50. Biekofsky RR, Martin SR, Browne JP, Bayley PM, Feeney J. Ca<sup>2+</sup> Coordination to Backbone Carbonyl Oxygen Atoms in Calmodulin and Other EF-Hand Proteins: <sup>15</sup>N Chemical Shifts as Probes for Monitoring Individual-Site Ca<sup>2+</sup> Coordination. *Biochemistry.* 1998; 37:7617–7629. [PubMed: 9585577]
51. Maguire ME, Cowan JA. Magnesium chemistry and biochemistry. *Biometals.* 2002; 15:203–210. [PubMed: 12206387]
52. Johnson C. X-ray crystal analysis of the substrates of aconitase. V. Magnesium citrate decahydrate [Mg(H<sub>2</sub>O)<sub>6</sub>][MgC<sub>6</sub>H<sub>5</sub>O<sub>7</sub>(H<sub>2</sub>O)]<sub>2</sub>·2H<sub>2</sub>O. *Acta Cryst.* 1965; 18:1004–1018. [PubMed: 14323450]
53. Diebler H, Eigen M, Ilgenfritz G, Maass G, Winkler R. Kinetics and mechanism of reactions of main group metal ions with biological carriers. *Pure Appl Chem.* 1969; 20:93–115.
54. Evenas J, Malmendal A, Thulin E, Carlstrom G, Forsen S. Ca<sup>2+</sup> binding and conformational changes in a calmodulin domain. *Biochemistry.* 1998; 37:13744–13754. [PubMed: 9753463]
55. Evenas J, Forsen S, Malmendal A, Akke M. Backbone dynamics and energetics of a calmodulin domain mutant exchanging between closed and open conformations. *J Mol Biol.* 1999; 289:603–617. [PubMed: 10356332]
56. Evenas J, Malmendal A, Akke M. Dynamics of the transition between open and closed conformations in a calmodulin C-terminal domain mutant. *Structure.* 2001; 9:185–195. [PubMed: 11286885]
57. Dupuis L, Mousseau N. Understanding the EF-hand closing pathway using non-biased interatomic potentials. *J Chem Phys.* 2012; 136:035101. [PubMed: 22280780]
58. Jurado LA, Chockalingam PS, Jarrett HW. Apocalmodulin. *Physiol Rev.* 1999; 79:661–682. [PubMed: 10390515]
59. Berridge MJ, Bootman MD, Lipp P. Calcium--a life and death signal. *Nature.* 1998; 395:645–648. [PubMed: 9790183]
60. Romani AM, Scarpa A. Regulation of cellular magnesium. *Front Biosci.* 2000; 5:D720–D734. [PubMed: 10922296]
61. Romani AM. Cellular magnesium homeostasis. *Arch Biochem Biophys.* 2011; 512:1–23. [PubMed: 21640700]
62. Brocard JB, Rajdev S, Reynolds IJ. Glutamate-induced increases in intracellular free Mg<sup>2+</sup> in cultured cortical neurons. *Neuron.* 1993; 11:751–757. [PubMed: 8104432]
63. Lee A, Zhou H, Scheuer T, Catterall WA. Molecular determinants of Ca(2+)/calmodulin-dependent regulation of Ca(v)2.1 channels. *Proc Natl Acad Sci U S A.* 2003; 100:16059–16064. [PubMed: 14673106]
64. Brunet S, Scheuer T, Klevit R, Catterall WA. Modulation of CaV1.2 channels by Mg<sup>2+</sup> acting at an EF-hand motif in the COOH-terminal domain. *J Gen Physiol.* 2005; 126:311–323. [PubMed: 16157690]

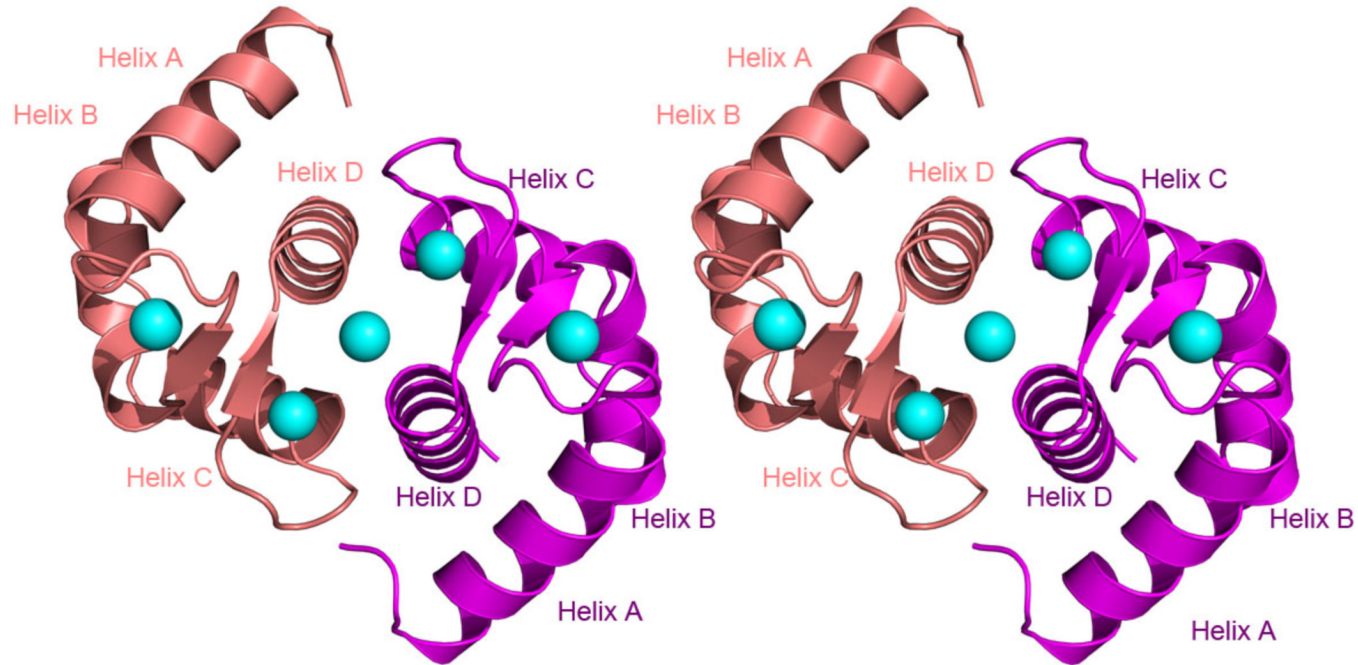
65. Rayssiguier Y, Mbega JD, Durlach V, Gueux E, Durlach J, Giry J, Dalle M, Mazur A, Laurant P, Berthelot A. Magnesium and blood pressure. I. Animal studies. *Magnes Res.* 1992; 5:139–146. [PubMed: 1390007]
66. Touyz RM. Role of magnesium in the pathogenesis of hypertension. *Mol Aspects Med.* 2003; 24:107–136. [PubMed: 12537992]
67. Touyz RM. Magnesium in clinical medicine. *Front Biosci.* 2004; 9:1278–1293. [PubMed: 14977544]
68. Weglicki W, Quamme G, Tucker K, Haigney M, Resnick L. Potassium, magnesium, and electrolyte imbalance and complications in disease management. *Clin Exp Hypertens.* 2005; 27:95–112. [PubMed: 15773233]
69. Mazur A, Maier JA, Rock E, Gueux E, Nowacki W, Rayssiguier Y. Magnesium and the inflammatory response: potential physiopathological implications. *Arch Biochem Biophys.* 2007; 458:48–56. [PubMed: 16712775]
70. Hsin K, Sheng Y, Harding MM, Taylor P, Walkinshaw MD. MESPEUS: a database of the geometry of metal sites in proteins. *Journal of Applied Crystallography.* 2008; 41:963–968.
71. DeLano, WL. The PyMOL Molecular Graphics System. Palo Alto, CA, USA: DeLano Scientific; 2002.



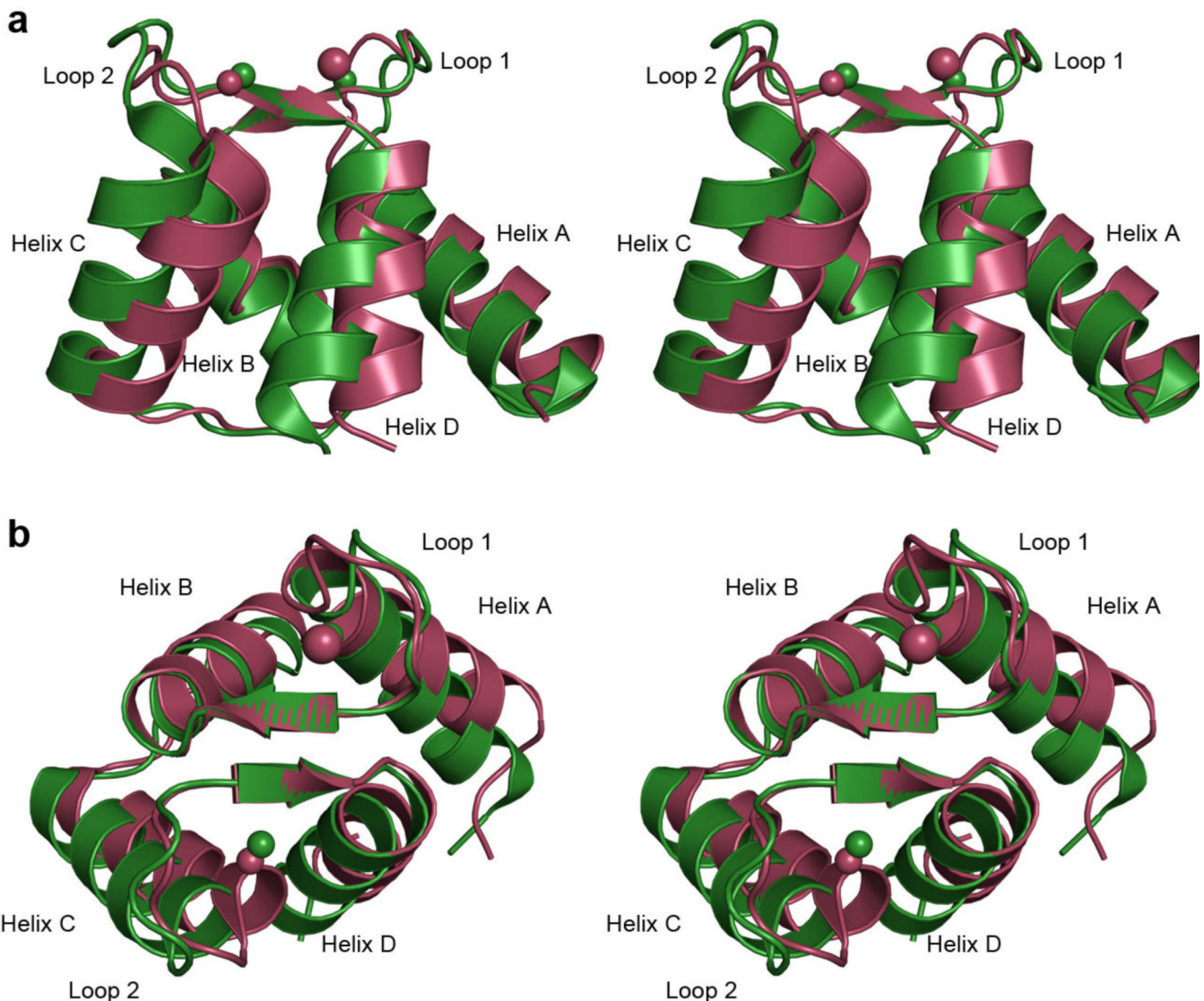
**Figure 1. Two modes of  $Mg^{2+}$  interaction with site II of N-CaM**

Stereo diagrams showing  $2Fo - Fc$  electron density maps contoured at  $1.5 \sigma$  and the corresponding atomic models for site II of N-CaM (residues 55–67).

(a) – The “final” state found in the tetragonal crystals of Mg/Zn-N-CaM. (b) – The “intermediate” state found in the monoclinic crystal of Mg-N-CaM. Note the difference in the position of the metal ion (cyan spheres) and in the number of water molecules (red spheres) retained by  $Mg^{2+}$ . In the intermediate state (b), the  $Mg^{2+}$  ion is directly coordinated to the N-CaM (blue lines) only via Thr62 side-chain and backbone carbonyl oxygen atoms. The remaining four coordinating positions are occupied by water molecules which make strong hydrogen bonds (yellow lines) with the side-chains of Asp58, Glu67 (each contributing two oxygen atoms), side-chain of Asp56, and the backbone carbonyl atom of Val55. A transition from the initial to the final position requires the elimination of two additional water molecules from the coordination sphere of  $Mg^{2+}$ , which are replaced by direct bonds to side-chain oxygen atoms of Asp56, Asp58 and Asn60. Two water molecules complete the octahedral ligand geometry around the  $Mg^{2+}$  ion, one of which forms a hydrogen bond to Glu67 at the C-terminal position of the loop. The only metal ligand contributed by the protein that is common to the two structures is the carbonyl oxygen of Thr62 (the –Y coordinating position), which belongs to the  $\beta$ -scaffold. All structure figures were prepared with Pymol (71).

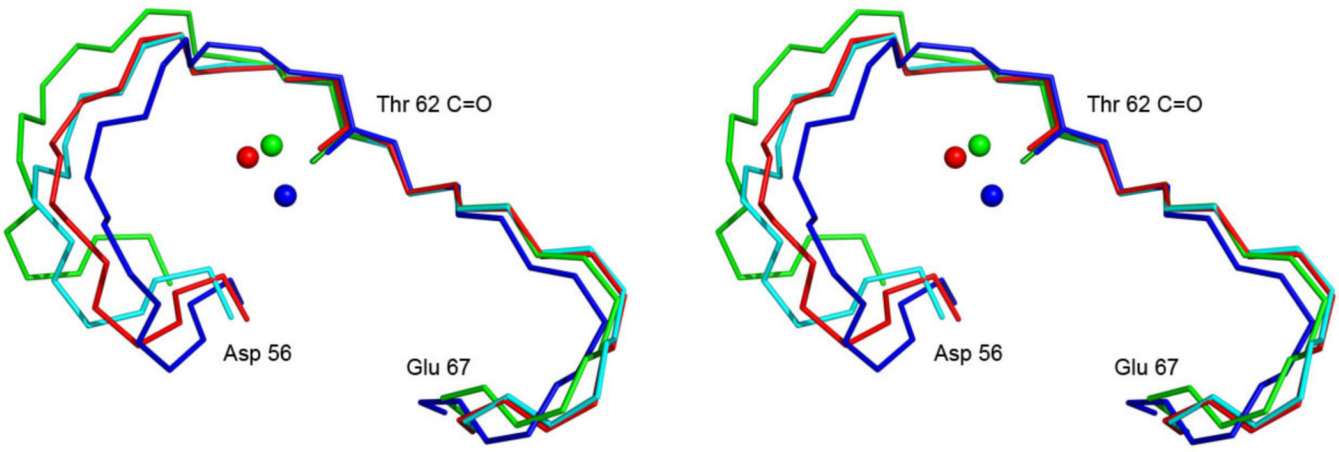


**Figure 2. Stereo view of the N-CaM dimer in the monoclinic crystal of Mg<sup>2+</sup>-N-CaM complex**  
Mg<sup>2+</sup> ions are shown as cyan spheres. Note the back-to-back interaction of N-CaM monomers involving EF-hand II and a Mg<sup>2+</sup> ion coordinated by the side chains of Asp64 (the residue in the 9<sup>th</sup> position of the loop). Due to the back-to-back interaction helix C is shifted and restricted in its movement.



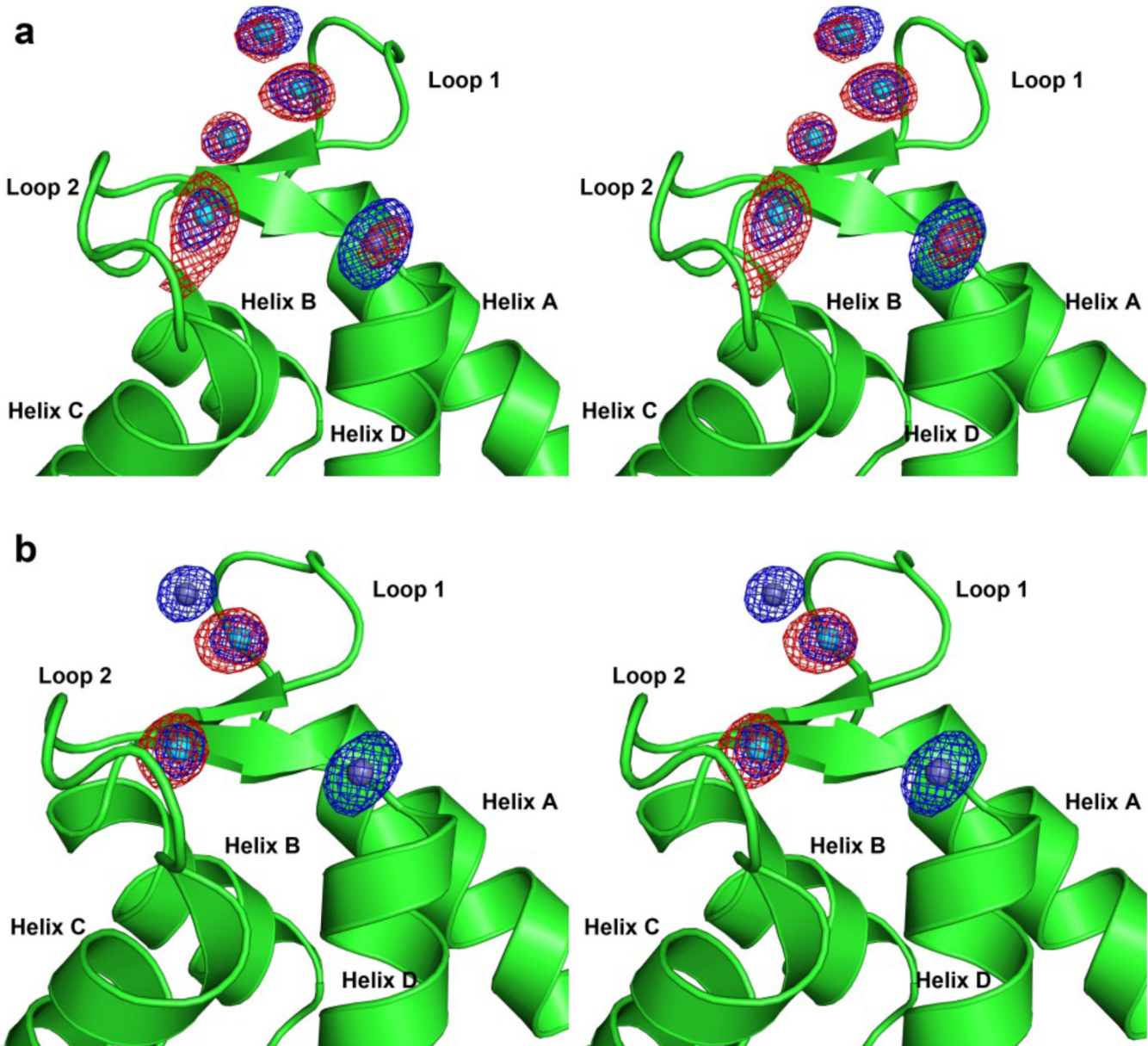
**Figure 3. Comparison of the domain structure of Mg-N-CaM and Mg/Zn-N-CaM**

The Mg-N-CaM is shown in green and the Mg/Zn-N-CaM is shown in red. Coordinates of the backbone atoms of the  $\beta$ -scaffold (Thr26, Ile27, Thr62, Ile63) were used for the superimposition. Note a large shift in the position of the entering helix of site II (helix C) in the Mg<sup>2+</sup>-N-CaM structure. Due to this shift the carbonyl oxygen of Val55 is approximately in the X coordinating position instead of Asp56 side-chain.

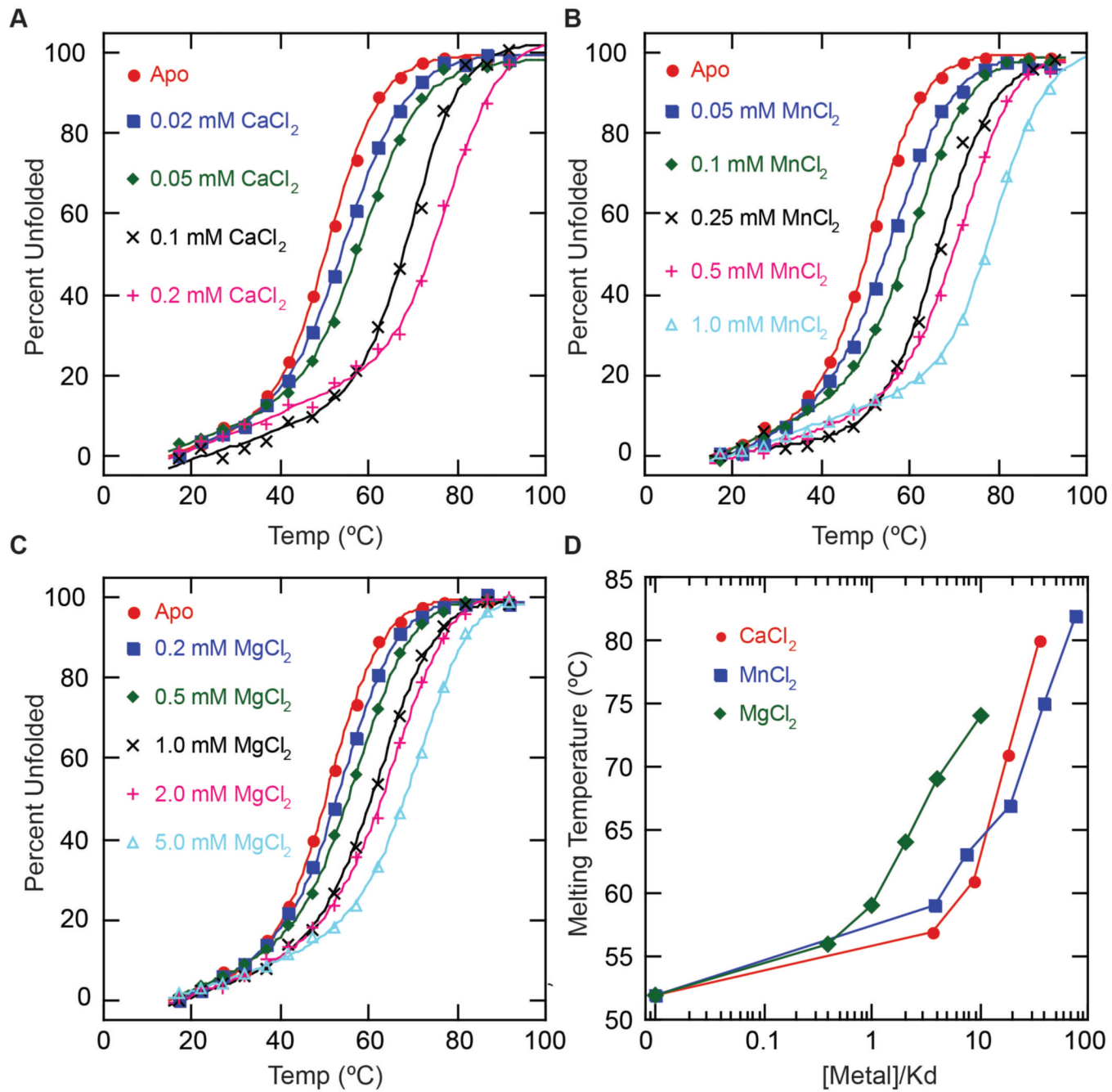


**Figure 4. Fluctuation of the EF-hand loop during metal ion binding**

A stereo diagram of the backbone structure of loop II of N-CaM (residues 56–67) is shown. Key: cyan - apo form (2PQ3), green – Mg-N-CaM (3UCW) featuring the transiently bound hydrated Mg<sup>2+</sup>, red – Mg/Zn-N-CaM (3UCY) the final position of dehydrated Mg<sup>2+</sup>, and blue - +Ca<sup>2+</sup> form (1CLL). Note that the loop initially expands to accommodate the hydrated Mg<sup>2+</sup> ion and then contracts to a similar conformation as the apo form when the H<sub>2</sub>O molecules are replaced by loop ligands (Supplementary Video). Further contraction of the loop occurs in the case of Ca<sup>2+</sup> when the bidentate Glu<sub>12</sub> engages in Ca<sup>2+</sup> coordination. The distance between Cα atoms of the first and last residue of the loop are: 8.6 Å (apo), 10.1 Å (hydrated Mg<sup>2+</sup>), 8.1 Å (Mg<sup>2+</sup>), and 6.6 Å (Ca<sup>2+</sup>).



**Figure 5. Identification of the bound  $Mn^{2+}$  and  $Zn^{2+}$  based on anomalous X-ray scattering**  
 The data were recorded at two wavelengths, 1.0750 Å (blue) and 1.7587 Å (red). The  $f'$  value for  $Zn^{2+}$  ions (dark blue spheres) is ~3 fold larger at the shorter wavelength when compared to the longer wavelength (2.83e and 0.92e, respectively), where the opposite is the case for  $Mn^{2+}$  ions (cyan spheres) (1.59e and 3.4e, respectively). **(a)** - chain A in which 4  $Mn^{2+}$  ions and 1  $Zn^{2+}$  ion are coordinated to the metal binding loops. **(b)** - chain B which binds 1  $Mn^{2+}$  ion and 1  $Zn^{2+}$  ions in each loop 1 and 2. Contours for the maps are  $6.0\sigma$  with a  $4.0\text{ \AA}$  cut-off around the metal. Sphere radii are reduced to  $0.5\text{ \AA}$  for both  $Mn^{2+}$  and  $Zn^{2+}$  to improve visibility.

**Figure 6. Stabilization of N-CaM structure by metal ions**

Melting profiles for N-CaM (in 10 mM Hepes, pH 7.5, 3 M urea) at various metal ion concentrations were determined by monitoring the circular dichroism signal at 222 nm for: A - Ca<sup>2+</sup>, B – Mn<sup>2+</sup> and C – Mg<sup>2+</sup>. When the increase in melting temperature is plotted as a function of [Me]/Kd the increase in stability induced by binding of each metal is similar as shown in D.

## Structure determination of N-CaM metal ion complexes.

**Table 1**

	Mg/Zn-N-CaM	Mg-N-CaM	Mn/Zn-N-CaM
<b>Data collection</b>			
Wavelength (Å)	1.0750	1.0750	1.0750
Space group	P4 <sub>3</sub> 2 <sub>1</sub> 2	P1	P2 <sub>1</sub>
Molecules in ASU	1	4	2
Cell dimension (Å)			
<i>a</i>	35.30	34.44	36.29
<i>b</i>	35.30	43.04	35.46
<i>c</i>	142.94	53.69	58.34
$\alpha$	90.00	68.45	90.00
$\beta$	90.00	88.62	93.12
$\gamma$	90.00	79.45	90.00
Resolution (Å)	1.8	1.76	1.90
R <sub>merge</sub> (%)	15.7 (59.2) <sup>d</sup>	7.1 (40.4) <sup>d</sup>	6.5 (33.5) <sup>d</sup>
I/σ (I)	18.3 (8.4) <sup>d</sup>	15.6 (2.7) <sup>d</sup>	28.7 (6.2) <sup>d</sup>
Completeness (%)	100.0 (100.0) <sup>d</sup>	95.6 (87.5) <sup>d</sup>	100 (99.9) <sup>d</sup>
Redundancy	27.4 (26.4) <sup>d</sup>	4.0 (3.3) <sup>d</sup>	8.2 (3.7) <sup>d</sup>
<b>Refinement</b>			
Unique reflections	9,179	27,732	11,882
R <sub>work</sub>	0.2023	0.198	0.204
R <sub>free</sub>	0.228	0.233	0.234
No. atoms			
Protein	575	2371	1150
Ligand/ion	9	10	10
Water	68	147	72
B-factors			
Protein	37.2	36.39	39.56
Ligand/ion	33.04	26.01	40.88
Water	50	35.65	41.94

	Mg/Zn-N-CaM	Mg-N-CaM	Mn/Zn-N-CaM
r. m. s. deviations			
Bond lengths (Å)	0.008	0.009	0.017
Bond angles (deg)	1.302	0.877	1.218
Ramachandran plot			
Favorable region	98.7	99.34	97.93
Allowed region	1.3	0.66	2.07
Disallowed region	0	0	0
Protein Data Bank ID	3UCY	3UCW	3UCT

All data sets were collected at NSLS Beamline X29.

<sup>a</sup>Outer resolution shell (1.86–1.80, 1.82–1.76, 1.97–1.90, 2.23–2.15, from left to right)

**Table 2**

Thermodynamic parameters of metal binding to N-CaM determined by isothermal titration calorimetry.

	<b>Ca<sup>2+</sup></b>	<b>Mn<sup>2+</sup></b>	<b>Mg<sup>2+</sup></b>
Number of sites	2.1 ± 0.1	2.0 ± 0.1	1.8 ± 0.2
K <sub>d</sub> (μM)	5.6 ± 0.1	13 ± 2	450 ± 10
ΔH (kcal/mol)	1.68 ± 0.06	3.8 ± 0.3	10 ± 1
ΔS (cal/mol °K)	29.7	34.9	48.7

**Table 3**Geometry of monodentate vs. bidentate coordination of Mg<sup>2+</sup>, Mn<sup>2+</sup> and Ca<sup>2+</sup>

Metal ion	Type of interaction	Bond distance		Bond angle		PDB ID (resolution, Å)
		O-Me (Å)	C-O-Me	O-Me-O		
Ca <sup>2+</sup>	monodentate	2.36 ± 0.05	138.0 ± 11.4	78.0 ± 2.4	1EXR (1.0)	
	bidentate	2.50 ± 0.06	92.7 ± 2.7	52.5 ± 0.8		
Mg <sup>2+</sup>	monodentate	2.08 ± 0.05	142.5 ± 14.6	90	3UCW (1.8)	
	bidentate <sup>a</sup>	2.33	89.9	56.7	1Z2O (1.24)	
Mn <sup>2+</sup>	monodentate	2.17 ± 0.04	139.5 ± 10.8	90	3UCT (1.9)	
	bidentate <sup>a</sup>	2.33	90.8	56.1	2W5T (1.6)	

<sup>a</sup>For Mg<sup>2+</sup> and Mn<sup>2+</sup> there are no examples of bidentate coordination among the published structures of EF-hand proteins. The examples given here are retrieved from PDB using MESPEUS server (70).